Advanced Materials Research Vols. 915-916 (2014) pp 1135-1139 *Online: 2014-04-09*

doi:10.4028/www.scientific.net/AMR.915-916.1135

Design Printable Pressure Sensor Based on 3DP Fabrication

LI Na [a], YANG Jiquan [b] and ZHOU Houyuan [c]

School of Electrical and Automation Engineering, Nanjing Normal University, China

[a]linananjing@163.com, [b]yangjiquang@njnu.edu.cn, [c]63053@njnu.eud.cn

Keywords: three Dimension Print (3DP), direct digital manufacturing (DDM), printable sensor, personal navigation.

Abstract. In this paper, a low cost, printable pressure sensor is presented. The pressure sensor will be used in personal navigation system which was designed based on micro jet fabrication structure. Inkjet printing and line patterning methods have been used to fabricate polymer resistors and field effect transistors on flexible substrates. A prototype sensor was designed, and the models of mechnical structure and ditital fabrication was also given, fabricated and tested with standard experimental measurements. Results verify that the pressure sensitivity can be measured for both requency and minimum power level difference in good perforamance. The dynamic performance of pressure sensor was also tested by inkjet printing on to flexible substrates including paper, with high resolution in just seconds.

Introduction

Research on MEMS pressure sensor has been concentrating in integration of sensing within the substrate for PNS (Personal Navigation System). The main goal is to get low cost, printable sensing capabilities. The benefit would be enhanced product quality, storage, transport and safety through ubiquitous sensing. A number of research groups have resulted in various printable sensor or actuator designs such as[1][2]: (i) Line based sensor (ii) pattern based (iii) R2R based etc. Fabrication progress makes it possible to produce more chipper sensor in large area with low requirement on substrate.

Pressure is one of most important physical parameters of measurement device such as navigation device for directing, electronic products for sensing, undersea vehicles[3] avoiding collisions with moving object, and so on. So the pressure sensors are used in many fields to better our lives. It became smaller in volume and higher in resolution. What we want to do is to design the printable sensor on to soft substrate， like coats，shoes， paper and plastic. Moreover, the printable sensor is flexible and able to fit inside various structures [5].

General theory of our proposed printable pressure sensor is detailed in the next section. The following section illustrates the design layout. In results section, a graphic description of the experimental procedure and corresponding measured data is presented.

Structure of the Printable Pressure Sensor

General theory of our proposed printable pressure sensor is detailed in this section. Also the resistor design is presented. The aim is to focus on pressure sensing mechanism in a printable structure.

The ratio of the change in resistance ΔR to the resistance R, called α, of a resistor in a material with piezoresistive coefficients π_i and stresses σ_i is

$$\alpha = \frac{\Delta R}{R} = \pi_l \sigma_l + \pi_t \sigma_t \tag{1}$$

where the subscripts *l* and *t* distinguish the longitudinal and transverse stresses with respect to the resistor length axis.

Consider Figure 1, which shows the placement of four resistors at the centers of the four edges of the surface of a square diaphragm with edge length L and thickness H.

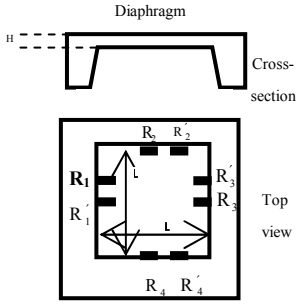

Figure 1: Four resistors at the centers of the four edges of the surface of a square diaphragm.

When a pressure P is applied from above the diaphragm, the diaphragm experiences stress and strain. As shown in [4] by finite-element methods (FEM), the stress (and strain) on the diaphragm is highest at the center of the edge, which we will call location DE, in the direction perpendicular to the edge:

$$\sigma \perp, DE, FEM = 0.243\left(\frac{L}{H}\right)^2 P \tag{2}$$

The strain in the parallel direction is

$$\in_{\parallel} = \frac{1}{E}\left(\sigma_{\parallel} - \nu\sigma_{\perp}\right). \tag{3}$$

Because the four edges are fixed, there is no strain in the direction parallel to cur edge anywhere along the edge, i.e. $\in_{\parallel}, edge = 0$. Thus, the stress at the center of an edge in the direction parallel to the edge is

$$\sigma_{\parallel}, DE, FEM = \nu\sigma_{\perp}, DE, FEM = 0.023\left(\frac{L}{H}\right)^2 P. \tag{4}$$

For a real resistor of resistance *R*, the overall relative change is the weighted average relative change of its infinitesimal components, integrating lengthwise:

$$\bar{\alpha} = \frac{1}{R}\int \alpha_{dR} dR = \frac{1}{R}\int_s \alpha_{dR}(s)\frac{\rho}{A(s)} ds \tag{5}$$

where *s* is the distance along the length of the resistor, ρ is the resistivity and A(s) is the cross-sectional area as a function of *s*.

The fabrication was layer by layer, as shown in Figure 2. This is a structure of heterogeneous object. Considering that the material distribution of functionally graded material objects is very complicated, only a union method to deal with material distribution with multi-references. The fabrication model is in next section.

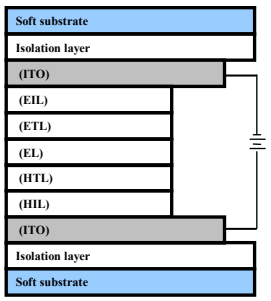

Figure 2 Sensor layered structure

3. Digital Model of the Printable Pressure Sensor

3.1. Three Dimension Printing. Three-dimensional printing is one of the DDM technologies that can be used for fabricating prototypes directly from CAD models in a layer-by-layer manner [4]. There

was a large variety of 3DP processes introduced in the past decade. In 3DP, successive layers of prototype are printed until the whole prototype is fabricated. Post-treatment of the prototype (such as infiltrating the part with other materials for strengthening or producing the part with the specified infiltrated material) will also be performed. There are numerous applications of 3DP, including model verification, functional testing, form and fit checking, etc. To produce heterogeneous or FGM prototypes, multiple printer heads will be introduced in the process and different materials and/or binders are deposited on different parts of the layers of the models. We design the controller to control both the inside and outside field to produce the drops in different resolution. In the first step the substrate was produced, and in the second step the devices was prototyped on it.

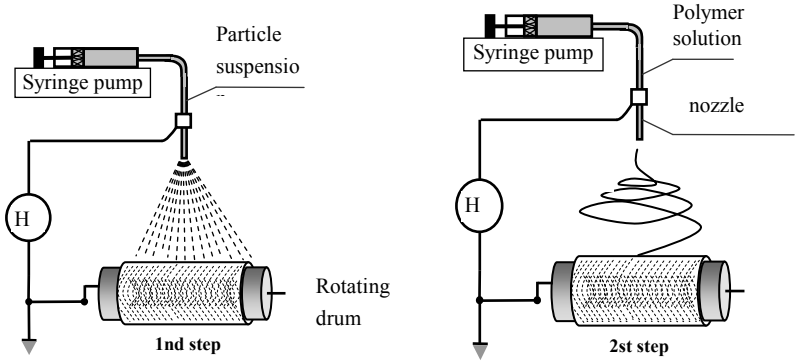

Figure 3 Fabrication progress

3.2. Color Models. To produce an attractive image, different colors must be applied. There are different color models available for representing colors [4] and different primary colors are employed. Some of them are RGB (red, green, blue), CMY (blue, red, yellow), HSB (hue, saturation, brightness), HLS (hue, lightness, saturation), and grey scale. By controlling the number of dots of each primary color, different resultant colors can be generated.

This can be done by mixing the corresponding color with white ink or screening the color into dots that are surrounded by white color, i.e. the more the white dots, the lighter the color [1]. Different colors are used as the primary colors of a color model.

For example, red, green, and blue are the primary colors of RGB, blue, red, and yellow are the primary colors of CMY, etc. In these color models, all colors are considered as a combination of different proportions of the primary colors of the corresponding model, for example, in RGB,

$$C_{ri} = \begin{bmatrix} x_{Ri} \\ x_{Gi} \\ x_{Bi} \end{bmatrix}_{RGB}$$

where xRi; xGi; xBi are the values of the primary colors and they represent the amount of red, green, and blue colors in the resultant color Cri of a pixel i. These values can be normalized and they are set as real numbers and, $0 \le x_{Ri}, x_{Gi}, x_{Bi} \le 1$.

In a RGB color model, a RGB color cube can be used to represent any combinations of these primary colors and any color is a point inside the color cube. The primary colors of RGB can be added to form secondary colors and these secondary colors are,

Red=Blue+Red; Blue=Green+Blue;Yellow=Red+Green.

Other primary and secondary colors combinations can be used to generate white color,

White=Blue┼Yellow; White=Green+Red;White=Red+Blue

The secondary colors can be used to form another color model CMY color model and the CMY color of a pixel *i* is

$$\begin{bmatrix} x_{Ci} \\ x_{Mi} \\ x_{Yi} \end{bmatrix} = \begin{bmatrix} 1 \\ 1 \\ 1 \end{bmatrix} - \begin{bmatrix} x_{Ri} \\ x_{Gi} \\ x_{Bi} \end{bmatrix}$$

In a printing process, a subtractive color model _ CMY is employed for managing the colors of different materials. Theoretically, heterogeneous can be generated by different materials. In this case, instead of a black color is introduced as a primary color and a CMY color model is employed in 3DP. To achieve the purpose of fabricating an FGM prototype, this CMY color model will be taken into consideration when planning the output data format of the model.

3.3. FGM model representation. To fabricate a prototype, it must first be represented in a CAD platform.

If the concentration of each primary color binder is diluted in different degrees, when a color prototype is fabricated, a nonhomogeneous or functionally graded one can be obtained. In general, a wider spectrum of binder concentration of a pixelm can be achieved by printing two binders with different concentrations in the appropriate proportion. To apply this concept for fabricating an FGM prototype, the proportion of the primary binders printed on different pixels of the object must be modeled so that varying binder concentration information can be obtained.

In the case of 3DP, only four primary binders are available (i.e, n= 4) and a tetrahedral binder concentration simplex is shown in Fig. 10(a). The colors of these primary binders are blue (B), red (R), yellow (Y), and clear (W) and their proportion vectors in the binder concentration simplex are denoted as $\mathbf{p}_1$,$\mathbf{p}_2$, $\mathbf{p}_3$,and $\mathbf{p}_4$ (corresponding to , $\mathbf{p}_C$, $\mathbf{p}_M$, $\mathbf{p}_Y$,and $\mathbf{p}_W$) respectively.

The corresponding sub-hyper-volume corresponding to $\mathbf{p}_m$ can be calculated as:

$$M_{sub-m1}=\begin{pmatrix}P_m\\P_2\\P_3\end{pmatrix},\quad M_{sub-m2}=\begin{pmatrix}P_m\\P_3\\P_1\end{pmatrix},\ M_{sub-m3}=\begin{pmatrix}P_m\\P_1\\P_2\end{pmatrix},\quad M_{Total}=\begin{pmatrix}P_1\\P_2\\P_3\end{pmatrix},$$

In general, the individual component (p_{mk}) of any point p_m is equal to the corresponding α_{mk} if the vertices of the binder concentration simplex (p_i) are unit vectors and mutually orthogonal to each other, i.e.

$$P_i=\begin{bmatrix}P_{i1} & P_{i2} & \cdots & P_{ij} & \cdots P_{im}\end{bmatrix} \text{ and } P_{ij}=\begin{cases}0 & \text{ifi}\neq j\\1 & \text{ifi}=j\end{cases} \tag{6}$$

Fabrication by Micro Jet 3DP

We design eight strain-gauge resistors on a square diaphragm in the pattern shown in Figure 1. The design exhibits odd symmetry about the center of the diaphragm, *i.e.* rotating it 180° yields an identical pattern, as shown in figure 4. The two resistors arranged in the center region change in the opposing direction as the two resistors arranged closer to the edges of the diaphragm. All eight resistors have narrower lines (10 μm for a 2000 μm diaphragm), which yields higher resistances, near the previously mentioned areas where absolute strain is high, and wider lines μm elsewhere. Since the ratios of lengths to widths remains constant, the resistance is scale-invariant.

This novel snaking resistor design is unnecessary for mast MEMS strain-gauge pressure sensors, which concentrate resistance on the high-strain regions of the diaphragm because the devices do not have wafer-scale conduction lines, but the additional resistance here more than compensates for the loss in sensitivity. As shown in Figure 4, the red line indicates the boundaries of the diaphragm (nominally 2000 μm), different microstructures can be molded by this process.

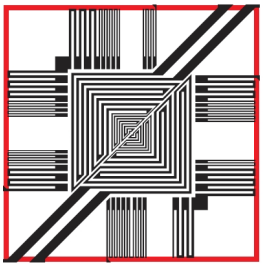

Figure 4: The design of four strain-gauge resistors on a square diaphragm.

The effect of the micro-structuring is best illustrated by a comparison of sensitivity and responsiveness of capacitive pressure sensors. One effect of the micro-structuring is a substantial increase in the device's response to the application of pressure.

Results

A. SENSITIVITY. Thermal noise voltage is on the order of:

$$V_N \approx \sqrt{4kTRf} \,. \tag{7}$$

where k is Boltzmann's constant, T is temperature, R is resistance, and f is the frequency. Thus, far T =300K , R =10 k Ω , and a filtered bandwidth of f = 100 Hz, the thermal noise voltage is approximately 0.13 μV . Therefore, the pressure resolution is on the order of 1.5 Pa. Object detection and identification requires only 10 Pa resolutions, so the strain-gauge pressure sensor is sufficiently sensitive for navigation applications.

B. Dynamics. The expected performance parameters for the strain-gauge pressure sensors of various diaphragm lengths L, as discussed in earlier sections of this paper, are summarized in Table 1. All diaphragms have thickness H=20 μm and all bridge source voltages are V_s=10V.

Note, however, that the performance parameters are subject to several factors, including the simplifications made to the deflection model, fabricated size of the diaphragm, and mask alignment. The performance was presented in Table 1.

Table 1: Expected performance parameters for strain-gauge pressure sensors

Diaphragm Length(μm)	1000	1414	2000	2828	4000
Ctr.Deflection c_1/P (nm/Pa)	0.0117	0.0471	0.189	0.742	3.11
Resistance (kΩ)	10	10	10	10	10
Sensitivity (μ V/Pa)	0.021	0.042	0.085	0.172	0.345
Noise (μ V)	0.14	0.15	0.14	0.15	0.15
Pressure Resolution (pa)	5.9	3.2	1.6	0.76	0.36
Pressure Range (MPa)	169	42.6	10.6	2.66	0.668
ResonantFrequency (kHz)	283	145	76	38	16

Acknowledgements

This work was financially supported by Natural Science Foundation of China (NSFC:61273243) and (NSFC:61304227).

References

[1] W.K. Chiu, Direct digital manufacturing of three-dimensional functionally graded material objects. Computer-Aided Design. Vol. 40 (2008), p. 1080-1903.

[2] Emran M. Amin, Nemai C. Karmakar, Development of A Low Cost Printable Humidity Sensor for Chipless RFID Technology, International Conference on RFID -Technologies and Applications (RFID - TA), 2012, p. 165-170.

[3] J. Virtanen, et al., "Inkjet-Printed Humidity Sensor for Passive UHF RFID Systems," Instrumentation and Measurement, IEEE Transactions on, vol. 60, 2011, p. 2768-2777.

[4] Nurdan Demirci Sankır, Flexible Electronics: Materials and Device Fabrication, Dissertation submitted to the Faculty of Virginia Polytechnic Institute and State University, 2005.

[5] Stephen Ming-Chang Hou, Design and Fabrication of MEMS-array Pressure sensor Navigation Inspired by Lateral line. Degree of Electronic Engineer MIT,2012.

Advanced Engineering Research
10.4028/www.scientific.net/AMR.915-916

Design Printable Pressure Sensor Based on 3DP Fabrication
10.4028/www.scientific.net/AMR.915-916.1135